The conversion is only valid if the two models are based on the same assumptions. This is not strictly true in the present case, because:

(i) the multipole analysis does allow for charge transfer between the two ions whereas the analysis based on $3d$ orbitals does not;

(ii) the assumption of tetragonal symmetry for the metallic ion surroundings instead of the true orthorhombic one was dropped in the multipole analysis.

However, the results obtained for P_{00} for both atoms show that there is no significant charge transfer. If the multiplicities of the atomic positions are taken into account, the values expected for P_{00} in the absence of charge transfer are 0·75 for Fe and 1·75 for the F atom. In fact,

$$P_{00}(\text{Fe}) = \text{number of } 3d \text{ electrons} \times \text{multiplicity}$$
$$= 6 \times 0{\cdot}125 = 0{\cdot}75$$

and

$$P_{00}(\text{F}) = \text{number of } (2s + 2p) \text{ electrons} \times \text{multiplicity}$$
$$= 7 \times 0{\cdot}25 = 1{\cdot}75.$$

Any increase in one of these values is bound to be accompanied by an equal decrease in the other so as to preserve unit-cell neutrality.

The occupancies of $3d$ orbitals of the Fe^{2+} ion derived from the multilpole population parameters using the appropriate matrix M are given in Table 5(*b*). The comparison of these results with those of Table 5(*a*) shows general agreement within one or (in a few cases) two standard deviations. However, the results derived from the multipole refinement (Table 5*b*) show a significant preference for the $d_{x^2-y^2}$ orbital, whereas those from the refinement of $3d$ occupancies indicate a slight preference for the d_{xy} orbitals. As fewer restrictions are imposed on the multipole model, its results might reproduce better the charge density in the real crystal. However, the conclusion that can be drawn from both models is the preference of the $3d$ electrons for the xy plane, together with a consequent depletion of the d_{z^2}, d_{xz} and d_{yz} orbitals.

We are indebted to the Cultural Service of the German Federal Republic Embassy, the Deutscher Akademischer Austauschdienst (DAAD) and the German Agency for Technical Cooperation (GTZ) for the offer of a CAD-4 automatic diffractometer which enabled the experimental work to be carried out.

References

ALMEIDA, M. J. M. DE & BROWN, P. J. (1988). *J. Phys. C*, **21**, 1111–1127.

ANDRADE, L. C. R. (1986). PhD Dissertation, Univ. of Coimbra, Portugal.

CLEMENTI, E. & ROETTI, C. (1974). *At. Data Nucl. Data Tables*, **14** (3), 4.

COSTA, M. M. R. & DE ALMEIDA, M. J. M. (1987). *Acta Cryst.* B**43**, 346–352.

FRENZ, B. A. (1983). *Enraf–Nonius Structure Determination Package; SDP Users Guide*, version 1.0. Enraf–Nonius, Delft, The Netherlands.

HANSEN, N. K. & COPPENS, P. (1978). *Acta Cryst.* A**34**, 909–921.

HOLLADAY, A., LEUNG, P. & COPPENS, P. (1983). *Acta Cryst.* A**39**, 377–387.

International Tables for X-ray Crystallography (1974). Vol. IV. Birmingham: Kynoch Press. (Present distributor Kluwer Academic Publishers, Dordrecht.)

NORTH, A. C. T., PHILLIPS, D. C. & MATHEWS, F. S. (1968). *Acta Cryst.* A**24**, 351–359.

STEVENS, E. D. & COPPENS, P. (1975). *Acta Cryst.* A**31**, 612–619.

STOUT, G. H. & JENSEN, L. H. (1968). *X-ray Structure Determination*, pp. 410–412. London: Macmillan.

Acta Cryst. (1989). B**45**, 555–562

Structure of the Incommensurately Modulated ε Phase of the Layered Perovskite $[NH_3(C_3H_7)]_2MnCl_4$ (PAMC) at 130 K

BY W. STEURER

Institut für Kristallographie und Mineralogie der Universität, Theresienstrasse 41, *D*-8000 *München* 2, *Federal Republic of Germany*

AND W. DEPMEIER

*Institut für Mineralogie und Kristallographie, BH*1, *TU Berlin, Ernst-Reuter-Platz* 1, *D*-1000 *Berlin* 12, *Federal Republic of Germany*

(*Received* 1 *August* 1988; *accepted* 1 *June* 1989)

Abstract

The incommensurately modulated structure of ε-PAMC has been determined at 130 K: bis-(*n*-propylammonium) tetrachloromanganate(II), M_r = 316·98, superspace group $P^{Abma}_{s11}[0,0{\cdot}363\ (2),0]$, a = 7·436 (4), b = 7·130 (6), c = 25·438 (12) Å, V = 1349 (2) Å^3, Z = 4, D_x = 1·56 Mg m^{-3}, Mo $K\bar{\alpha}$,

0108-7681/89/060555-08$03.00

$\lambda = 0{\cdot}71069$ Å, $\mu = 1{\cdot}75$ mm^{-1}, $F(000) = 652$, $wR(F) = 0{\cdot}050$ for 1747 independent reflections, $wR(F) = 0{\cdot}072$ for 1135 first-order satellites. The interpretation of the results relies strongly on (3 + 1)-dimensional electron density maps. The characteristics of the modulated structure including the components and magnitudes of the modulation functions of the different atoms, their mutual non-symmetry-related phase relationships and their temperature dependence are explained by an atomistic model. The model is based on the assumption of hindered freezing of the dynamical disorder of the propylammonium ions and of the associated hydrogen-bonding system. The hindrance is thought to be due to the existence of a relatively rigid interlayer of terminal methyl groups belonging to adjacent layers.

Introduction

The title compound, bis(*n*-propylammonium) tetrachloromanganate(II) (PAMC), belongs to a large structural family of general formula $(C_nH_{2n+1}NH_3)_2MX_4$ with $M = Mn^{2+}$, Cd^{2+}, Fe^{2+}, Cu^{2+}, Cr^{2+}, Pd^{2+}, and $X = Cl^-$ or Br^-. This group was initially studied because of pronounced two-dimensional magnetism in the case of magnetic cations. Later, more and more interest was raised by the structural phase transitions encountered in the various members of the family. Thus, PAMC played a particular role, because of its peculiar sequence of phases, with the occurrence of two incommensurately modulated phases and two hitherto unknown types of incommensurate–commensurate phase transitions. The properties and the scientific history of PAMC have been reviewed recently (Depmeier, 1986).

It is perhaps useful to recall the most important features of the structure of PAMC (and its homologues). Layers of corner-sharing MX_6 octahedra are sandwiched between layers of $C_nH_{2n+1}NH_3$ groups, which are attached to the former *via* N—H···Cl hydrogen bonds. The octahedra layers resemble (100) slabs of perovskites and this is the reason why the term 'layered perovskites' has become customary. At elevated temperatures the $C_nH_{2n+1}NH_3$ groups are dynamically disordered; decreasing temperatures cause gradual freezing of these groups. At room temperature the dynamical disorder is usually restricted to a librational movement of these groups across a mirror plane m_y. For PAMC it has been shown that the dynamical disorder of the C_3H_7 residues persists down to the $\varepsilon \rightarrow \zeta$ phase transition at 112·5 K, whereas the proton interchange within the $—NH_3$ group exists down to about 100 K, where it dies out (Muralt, 1984). The present paper will deal with the structure of the incommensurately modulated ε phase, which is stable between 168 and 112·5 K (Brunskill & Depmeier, 1982).

Experimental

Crystals of PAMC were grown from aqueous solutions of stoichiometric $MnCl_2$ and $C_3H_7NH_3Cl$. Several crystals had to be tested before a suitable one was found which was not damaged or destroyed by the freezing of solvent inclusions on cooling. The crystal, of approximate dimensions 0·1 × 0·1 × 0·05 mm, was fixed with a touch of silicon grease in a glass capillary and mounted on a Syntex *R*3 diffractometer equipped with a cold-stream low-temperature device. Data collection: graphite monochromator, $\lambda = 0{\cdot}71069$ Å, lattice parameters from centring 25 strong main reflections; because the deviation from commensurability is small (Depmeier & Mason, 1982, 1983) PAMC was treated as a threefold superstructure with $b' = 3b$ for data collection; $(\sin\theta/\lambda)_{max} = 0{\cdot}60$ Å^{-1}, $0 \le h \le 9$, $0 \le k' \le 26$, $-31 \le l \le 31$; temperature estimation (130 K) from strongly temperature-dependent *c*-lattice parameter and comparison with neutron data (Depmeier & Mason, 1982); constancy of temperature checked by using satellite reflections with strongly temperature-dependent intensities (Depmeier & Mason, 1983) as standards, only small drift to slightly higher temperatures during the experiment; ω scans, variable scan speed 2–12° min^{-1}; Lorentz and polarization corrections, empirical absorption correction; 3897 reflections measured, 1747 independent reflections after averaging and elimination of space-group-forbidden reflections.

Structure determination: the symmetry of the ε phase of PAMC was determined by Brunskill & Depmeier (1982). From the reflection conditions, *hklm*: $k + l = 2n$, 0*klm*: $k + m = 2n$ and *hk*0*m*: $h = 2n$, the superspace group $P^{Abma}_{s\,11}(0,\frac{1}{3}+\delta,0)$ [No. 64*c*.15.2 in the table of superspace groups of de Wolff, Janssen & Janner (1981)] was derived. The non-standard setting for the space group of the basic (= average) structure was chosen with the intention of emphasizing the group–subgroup relationship between the symmetries of the high- and low-temperature phases [*cf.* Table 1 of Depmeier (1986)]. The superspace group as given above generates from the general position (x, y, z, t') the equivalent one with coordinates $(-x, -y, -z, \frac{1}{2}-t')$; hence, the centre of symmetry does not coincide with the origin. Therefore, the transformation $t = t' - \frac{1}{4}$ was performed. The coordinates of the 16-fold general position obtained were: $(0, 0, 0, 0; 0, \frac{1}{2}, \frac{1}{2}, 0) + \{\pm(x, y, z, t); \pm(\frac{1}{2}-x, \frac{1}{2}+y, z, \frac{1}{2}+t); \pm(x, -y, z, \frac{1}{2}-t); \pm(\frac{1}{2}+x, y, \frac{1}{2}-z, t)\}$.

Since only first-order satellite reflections were observed, it was possible to use simple harmonic

modulation functions for the description of the periodic deviations of the actual structure from the basic structure. Modulations of the atomic positional and 'thermal' parameters were taken into account. Thus, the kth symmetrically independent atom was described by three component modulation waves of the form $u_k(t) = u_k^0 + u_k^c\cos 2\pi t - u_k^s\sin 2\pi t$, $v_k(t) = v_k^0 + v_k^c\cos 2\pi t - v_k^s\sin 2\pi t$, $w_k(t) = w_k^0 + w_k^c\cos 2\pi t - w_k^s\sin 2\pi t$, with u, v, w referring to the x, y and z directions, respectively. The coordination characteristics of individual atoms could be expected to vary periodically with the positional modulation with consequent implications for the state of the static or dynamic disorder of the $MnCl_6$ octahedra and $C_3H_7NH_3$ groups. The suitable way to describe these effects is to use modulated 'temperature factors'. The coefficients of the modulated anisotropic 'temperature factors' are given as $U_{ij}^k(t) = U_{ij}^{0,k} + U_{ij}^{c,k}\cos 2\pi t - U_{ij}^{s,k}\sin 2\pi t$ with $1 \le i,j \le 3$. Special positions required symmetry restrictions on some modulation parameters. These are shown in Table 1.

The average structure has been refined in the space group *Abma*, with the values of the δ phase of PAMC (Depmeier & Mason, 1978) as starting parameters. Both structures agree closely with each other. Owing to the inherent high dynamical disorder of the propylammonium (PAM) group, also confirmed by spectroscopic methods (*cf.* Depmeier, 1986), this group had to be refined with a split-atom model. The split PAM groups are related by the m_y mirror plane. The R factors were $R = 0{\cdot}048$ and $wR = 0{\cdot}048$ for 612 main reflections and 63 variables.

In the first stage of the refinement of the modulated structure only the modulation parameters of Mn, Cl(1) and Cl(2) were allowed to vary. The R factor for the satellite reflections thus obtained was $wR = 0{\cdot}277$. Subsequently, three different models were tested. The first one consisted of a modulation of the occupancy factors of the PAM split positions. Such a modulation would be caused by a coupled, periodically alternating occupation of the split positions. The corresponding satellite R factor was $wR = 0{\cdot}236$. In the second model, the PAM cation was placed on the mirror plane $(\frac{m}{1})_y$ and refined with harmonic modulation functions for the positional and 'thermal' parameters of the atoms. The wR value dropped to 0·149. The third model converged to $wR = 0{\cdot}089$. It described the modulated PAM group by two split molecules, generated by displacing the PAM group slightly from the mirror plane, with individual shift modulation functions for each split atom. An analysis of the (3 + 1)-dimensional electron density maps (*cf.* Steurer, 1987) suggested that, in addition, modulated 'thermal' parameters for at least the PAM split atoms should be refined. A significant decrease of wR to a value of 0·082 confirmed the correctness of this assumption. In the final stages the modulated 'temperature factors' of all atoms were released and the final R factors were $R = 0{\cdot}056$ and $wR = 0{\cdot}050$ for all 1747 reflections (including unobserved ones) and 139 variables. Partial R factors were $R = 0{\cdot}043$ and $wR = 0{\cdot}046$ for 612 main reflections, and $R = 0{\cdot}091$ and $wR = 0{\cdot}072$ for 1135 first-order satellites. Weights $w(F) = \sigma^{-2}(F)$ were applied and the bonds N—C(1), C(1)—C(2) and C(2)—C(3) were subjected to soft constraints. The corresponding bond lengths were set to 1·48, 1·53 and 1·53 Å, respectively, and a small variation of ±0·02 Å during a modulation period for each of the bonds was allowed, thus accounting for the periodically changing virtual shortening of the bonds resulting from the librational motion of the atoms (*cf.* Willis & Pryor, 1975). During all refinements the H atoms were constrained to ride on the atoms they are bonded to. The calculations were performed with the programs *SHELXTL* (Sheldrick, 1978) for the average structure and *REMOS* (Yamamoto, 1982*a*,*b*) for the modulated structure. Atomic scattering factors were taken from *International Tables for X-ray Crystallography* (1974). $\Delta/\sigma_{max} = -0{\cdot}21$ for the average structure, 0·02 for the modulated structure.

Table 1. *Symmetry restrictions on the coordinates and modulation parameters for the atoms on special sites*

In each case, the first three rows list the displacive-modulation parameters, u_k^0, u_k^c, u_k^s *etc.*, the following six rows contain the thermal-modulation parameters $U_{ij}^{0,k}$, $U_{ij}^{c,k}$, $U_{ij}^{s,k}$.

Mn on $(\frac{2}{s})_y/(\frac{m}{s})_y$			Cl(1) on $(\frac{2}{1})_z$			Cl(2) on $(\frac{m}{s})_y$		
0	0	u_{Mn}^c	$\frac{1}{4}$	0	$u_{Cl(1)}^c$	$u_{Cl(2)}^0$	0	$u_{Cl(2)}^c$
0	0	0	$\frac{1}{4}$	0	$v_{Cl(1)}^c$	0	$v_{Cl(2)}^c$	0
0	0	w_{Mn}^c	$w_{Cl(1)}^0$	$w_{Cl(1)}^c$	0	$w_{Cl(2)}^0$	0	$w_{Cl(2)}^c$
U_{11}^0	0	0	U_{11}^0	U_{11}^c	0	U_{11}^0	0	U_{11}^s
U_{22}^0	0	0	U_{22}^0	U_{22}^c	0	U_{22}^0	0	U_{22}^s
U_{33}^0	0	0	U_{33}^0	U_{33}^c	0	U_{33}^0	0	U_{33}^s
0	U_{12}^c	0	U_{12}^0	U_{12}^c	0	0	U_{12}^c	0
U_{13}^0	0	0	0	0	U_{13}^s	U_{13}^0	0	U_{13}^s
0	U_{23}^c	0	0	0	U_{23}^s	0	U_{23}^c	0

Results and discussion

Refined atomic parameters including the Fourier coefficients of the component modulation waves are given in Table 2.* The maximum shifts from the average positions are about 0·1 to 0·2 Å for the atoms of the $MnCl_6$ octahedra and up to 0·35 Å for those of the PAM group. The 'thermal' parameters are higher than usually encountered at 130 K, thus demonstrating the high degree of inherent static and/or dynamic disorder of both the inorganic [$U_{33}^{0,Mn} = 0{\cdot}036$ (1), $U_{22}^{0,Cl(2)} = 0{\cdot}046$ (1) Å^2, *etc.*] and

* A list of structure factors and Figs. 4–6 have been deposited with the British Library Document Supply Centre as Supplementary Publication No. SUP 52007 (28 pp.). Copies may be obtained through The Executive Secretary, International Union of Crystallography, 5 Abbey Square, Chester CH1 2HU, England.

Table 2. *Fractional displacive atomic modulation amplitudes* u_k^0, u_k^c, u_k^s, ... ($\times 10^4$) *and modulation parameters* $U_{ij}^{0,k}$, $U_{ij}^{c,k}$, $U_{ij}^{s,k}$ *of the anisotropic temperature factors* (Å $\times 10^3$) *with e.s.d.'s in parentheses*

The numbers in the first column correspond to the atomic parameters of the basic structure, the second column gives the amplitudes of the cosine terms and the third column those of the sine terms of the modulation functions.

Mn	$u_{Mn}(t)$	0	0	−7 (1)
	$v_{Mn}(t)$	0	0	0
	$w_{Mn}(t)$	0	0	36 (1)
	$U_{11}(t)$	14 (1)	0	0
	$U_{22}(t)$	24 (1)	0	0
	$U_{33}(t)$	36 (1)	0	0
	$U_{23}(t)$	0	0 (1)	0
	$U_{12}(t)$	0	0 (1)	0
Cl(1)	$u_{Cl(1)}(t)$	¾	0	14 (1)
	$v_{Cl(1)}(t)$	¾	0	16 (1)
	$w_{Cl(1)}(t)$	5103 (1)	50 (1)	0
	$U_{11}(t)$	18 (1)	0	0
	$U_{22}(t)$	27 (1)	0	0
	$U_{33}(t)$	45 (1)	0	0
	$U_{23}(t)$	0	0	0 (1)
	$U_{13}(t)$	0	0	0 (1)
	$U_{12}(t)$	2 (1)	0	0
Cl(2)	$u_{Cl(2)}(t)$	472 (1)	0	28 (1)
	$v_{Cl(2)}(t)$	0	−277 (1)	0
	$w_{Cl(2)}(t)$	963 (1)	0	34 (1)
	$U_{11}(t)$	20 (1)	0	0 (1)
	$U_{22}(t)$	44 (1)	0	7 (1)
	$U_{33}(t)$	36 (1)	0	0 (1)
	$U_{23}(t)$	0	0 (1)	0
	$U_{13}(t)$	0 (1)	0	0 (1)
	$U_{12}(t)$	0	0 (1)	0
N	$u_N(t)$	−242 (5)	−4 (33)	−24 (5)
	$v_N(t)$	−101 (15)	−194 (7)	−181 (25)
	$w_N(t)$	4143 (1)	−59 (6)	−8 (1)
	$U_{11}(t)$	20 (2)	6 (8)	0 (2)
	$U_{22}(t)$	53 (4)	48 (6)	−26 (6)
	$U_{33}(t)$	22 (1)	6 (3)	−3 (1)
	$U_{23}(t)$	−1 (1)	−3 (1)	−11 (3)
	$U_{13}(t)$	0 (1)	0 (1)	0 (1)
	$U_{12}(t)$	−3 (2)	−2 (1)	7 (3)
C(1)	$u_{C(1)}(t)$	744 (7)	91 (27)	−53 (6)
	$v_{C(1)}(t)$	310 (13)	107 (12)	80 (12)
	$w_{C(1)}(t)$	3660 (1)	−28 (5)	1 (1)
	$U_{11}(t)$	29 (3)	−19 (10)	3 (3)
	$U_{22}(t)$	35 (7)	−24 (7)	7 (6)
	$U_{33}(t)$	42 (1)	−36 (7)	0 (1)
	$U_{23}(t)$	−1 (1)	9 (2)	0 (1)
	$U_{13}(t)$	2 (1)	0 (3)	0 (1)
	$U_{12}(t)$	3 (1)	−16 (4)	−3 (1)
C(2)	$u_{C(2)}(t)$	−149 (7)	9 (26)	310 (8)
	$v_{C(2)}(t)$	−358 (19)	−256 (15)	−361 (20)
	$w_{C(2)}(t)$	3175 (1)	31 (6)	−4 (1)
	$U_{11}(t)$	41 (3)	−15 (12)	15 (4)
	$U_{22}(t)$	111 (11)	−81 (21)	−24 (7)
	$U_{33}(t)$	36 (1)	−13 (7)	0 (1)
	$U_{23}(t)$	0 (2)	1 (3)	−1 (2)
	$U_{13}(t)$	0 (1)	−2 (3)	0 (1)
	$U_{12}(t)$	−19 (3)	8 (5)	1 (3)
C(3)	$u_{C(3)}(t)$	933 (7)	−160 (37)	303 (10)
	$v_{C(3)}(t)$	−114 (28)	−18 (11)	60 (34)
	$w_{C(3)}(t)$	2686 (1)	15 (8)	16 (2)
	$U_{11}(t)$	49 (4)	17 (11)	39 (7)
	$U_{22}(t)$	65 (6)	−19 (12)	20 (9)
	$U_{33}(t)$	45 (1)	29 (7)	0 (3)
	$U_{23}(t)$	9 (2)	4 (1)	9 (3)
	$U_{13}(t)$	4 (1)	2 (3)	0 (1)
	$U_{12}(t)$	1 (4)	−8 (3)	−2 (5)

the organic [$U_{22}^{0,C(2)} = 0{\cdot}112\,(9)$ Å^2, *etc.*] structural components. Graphic representations of the rather abstract numbers of Table 2 are shown in Figs. 1–3, additional figures have been deposited.† A first impression of the character of the modulation is provided by Fig. 1(*a*). It illustrates, in a projection of the crystal structure onto the *bc* plane, the main structural distortions which are caused by the modulation with $\mathbf{q} \| \mathbf{b}^*$. In particular, a tilt of the $MnCl_6$ octahedra, about axes parallel to the *x* direction, becomes noticeable. The maximum tilt angle is ±5°. The split PAM molecules change their conformations and positions from a complete coincidence to a significant separation [about 1·4 Å for the C(2) split atoms] within one modulation period. For the sake of clarity the modulation of the 'thermal' parameters has been ignored in this drawing. The corresponding refined values should not be taken too literally though, because, in combination with the split model, they have to be understood as being more or less mere fit parameters of the periodically changing dynamical smearing of the PAM group (and also of the $MnCl_6$ octahedra), rather than describing physical reality exactly. Figs. 1(*b*) and 1(*c*) show the shifts of the structural building elements in the other directions. However, it should be noted that the conspicuous washboard-like puckering along **a** of the perovskite layers is not due to the modulation, but is a result of the N—H···Cl hydrogen bonds (Depmeier & Mason, 1978). The puckering is one of the major structural features of the basic structure (δ-PAMC). As far as the perovskite-type layers are concerned, Figs. 1(*a–c*) demonstrate convincingly that the modulation acts merely as a small perturbation on the basic structure.

The description of the modulated structure by an *ORTEP* plot is certainly useful for getting a conceptual idea of the modulation. However, more detailed information can only be obtained from the electron density function itself. Figs. 2 and 3 show bounded projections of the (3 + 1)-dimensional Fourier functions (*cf.* Steurer, 1987) for the atoms Cl(1), Cl(2), N, C(1), C(2) and C(3). They allow the following observations to be made:

(i) The *y*-component modulation amplitudes of Cl(2) and N are both large and roughly equal in magnitude. These longitudinal modulation waves destroy the m_y mirror planes of the space group of the basic (average) structure. Pairs of N and Cl(2) atoms, which have similar *x* parameters and *y* parameters that differ by 0·5 in the basic structure, have modulation waves which are *in antiphase* (Fig. 3). A slight increase (decrease) of the electron density is observed in regions where N and Cl(2) approach (move away from) each other. These regions overlap

† See deposition footnote.

with the loci of H(2) atoms, which were identified by neutron diffraction (Depmeier & Mason, 1978).

(ii) The *y*-component modulation wave of C(3) has practically zero amplitude (Fig. 3*f*).

(iii) The *x*-component modulation amplitude is negligible for Cl(2) and N, but large for C(3) (Fig. 2).

(iv) The modulation waves of C(1) and C(2) have important components in the *x* as well as in the *y* direction. The amplitudes are quite large and the waves are rather irregularly shaped [variation of 'temperature factor', Fig. 3(*d*), and splitting, Fig. 3(*e*)].

(v) The *y*-component wave of N and the *x*-component wave of C(3), both atoms being in the same PAM group, are *in quadrature* (phase shift of $\sim\pi/2$, Figs. 2*e*, 3*c*).

(vi) C(3) atoms, which belong to a given stratum ($z\simeq 0{\cdot}23$) or to an adjacent one ($z\simeq 0{\cdot}27$) are all *in phase* [see Fig. 4 (deposited), *cf.* also Fig. 7 of Depmeier (1979)].

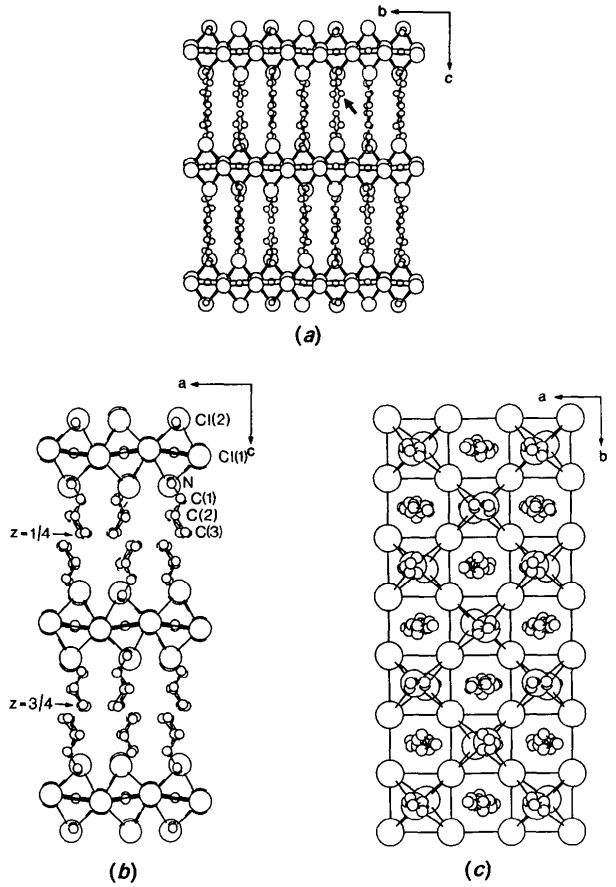

Fig. 1. *ORTEP* plots (Johnson, 1965) of the crystal structure of ε-PAMC extending over one modulation period. The atoms are shown as circles with radii proportional to the ionic or atomic radii (the H atoms are omitted). The PAM group is plotted according to the split-molecule model. This means that the split atoms are related by the $(\frac{m}{\uparrow})_y$ mirror planes in $y = 0, \frac{1}{2}, \ldots$ The projection down **a** is given in (*a*), illustrating clearly the modulation principles. The tilting of the octahedra around **a** and the varying deviation of the PAM group from mirror symmetry (an especially large deviation is marked by an arrow) can be seen. The projection down **b** is plotted in (*b*) and down **c** in (*c*). The origin is always in the center of the octahedron at the upper right corner.

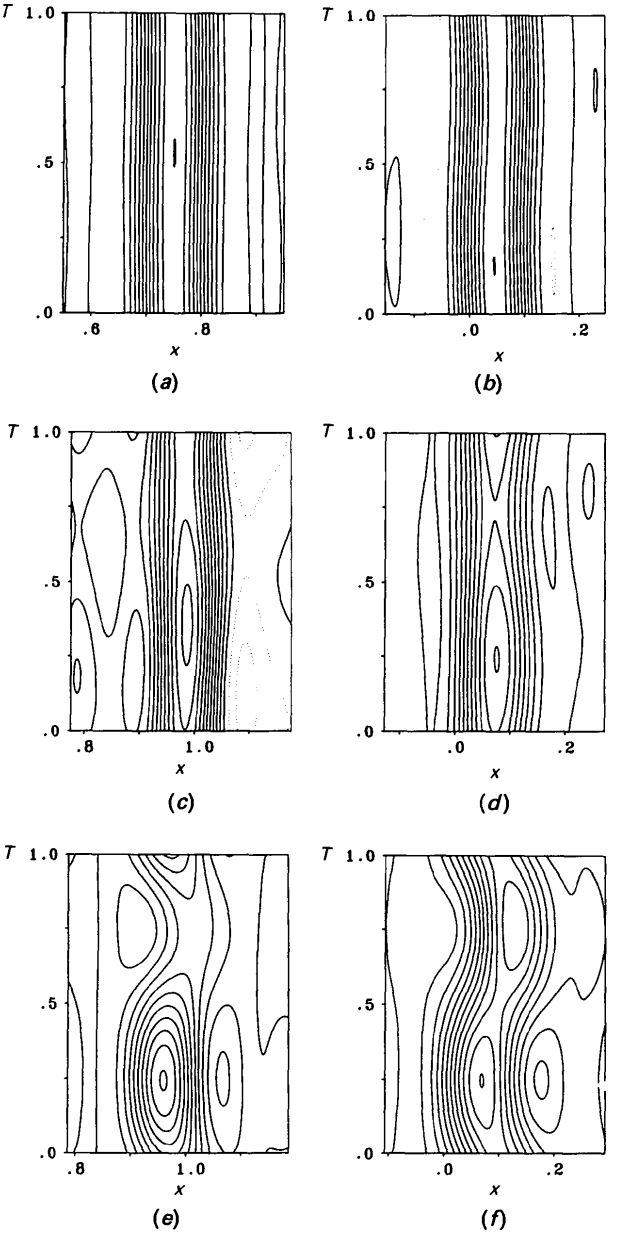

Fig. 2. Bounded projections of the (3 + 1)-FF of ε-PAMC parallel to the *xt* plane. The maps show the modulation functions $u_k(t) = u_k^c\cos 2\pi t - u_k^s\sin 2\pi t$ of the atoms of the PAM molecule. (*a*) Cl(1) within $0{\cdot}7 \le y \le 0{\cdot}8$, $0{\cdot}5003 \le z \le 0{\cdot}5203$; (*b*) Cl(2) within $-0{\cdot}05 \le y \le 0{\cdot}05$, $0{\cdot}0863 \le z \le 0{\cdot}1063$; (*c*) N within $-0{\cdot}05 \le y \le 0{\cdot}05$, $0{\cdot}4043 \le z \le 0{\cdot}4243$; (*d*) C(1) within $-0{\cdot}05 \le y \le 0{\cdot}05$, $0{\cdot}3554 \le z \le 0{\cdot}3754$; (*e*) C(2) within $-0{\cdot}05 \le y \le 0{\cdot}05$, $0{\cdot}3084 \le z \le 0{\cdot}3284$; (*f*) C(3) within $-0{\cdot}0441 \le y \le 0{\cdot}0559$, $0{\cdot}2585 \le z \le 0{\cdot}2785$.

Further useful results can be obtained from Table 2 and its evaluation:

(vii) The z components of all modulation waves are small or insignificant.

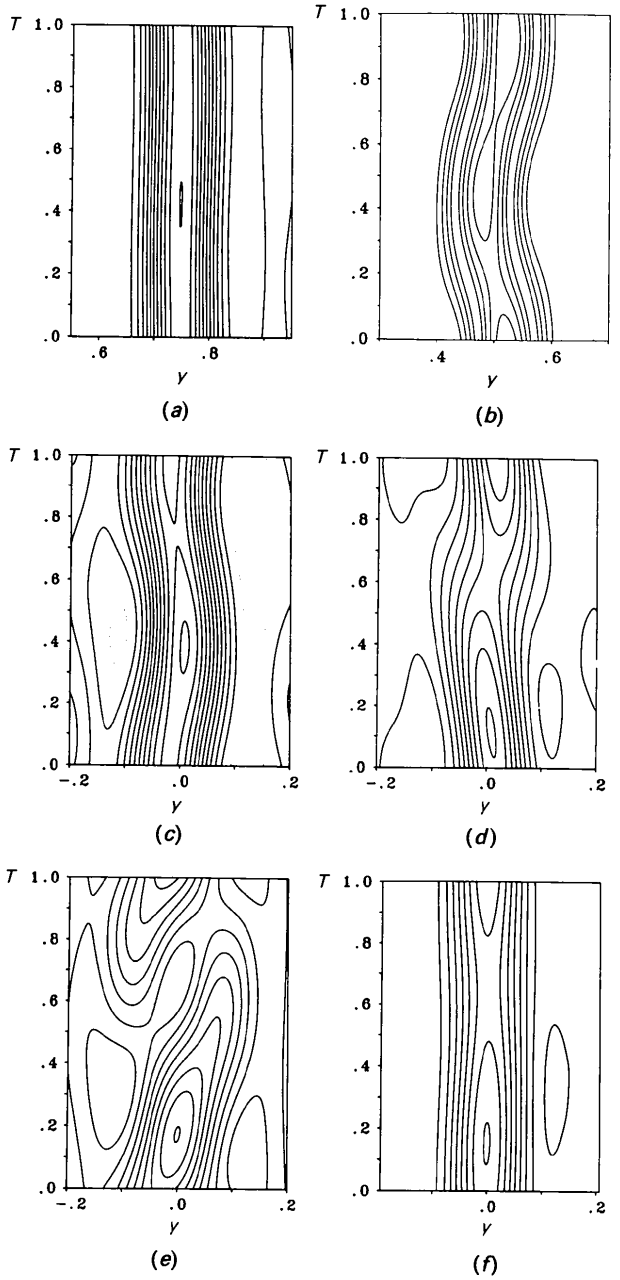

Fig. 3. Bounded projections of the (3 + 1)-FF of ε-PAMC parallel to the yt plane. The maps show the modulation functions $v_k(t) = v_k^c\cos 2\pi t - v_k^s\sin 2\pi t$ of the atoms of the PAM molecule. (*a*) Cl(1) within $0{\cdot}7 \le x \le 0{\cdot}8$, $0{\cdot}5003 \le z \le 0{\cdot}5203$; (*b*) Cl(2) within $-0{\cdot}0972 \le x \le 0{\cdot}0028$, $0{\cdot}3937 \le z \le 0{\cdot}4137$; (*c*) N within $0{\cdot}9264 \le x \le 1{\cdot}0264$, $0{\cdot}4042 \le z \le 0{\cdot}4243$; (*d*) C(1) within $0{\cdot}0221 \le x \le 0{\cdot}1221$, $0{\cdot}3554 \le z \le 0{\cdot}3754$; (*e*) C(2) within $0{\cdot}9364 \le x \le 1{\cdot}0364$, $0{\cdot}3084 \le z \le 0{\cdot}3284$; (*f*) C(3) within $0{\cdot}0423 \le x \le 0{\cdot}1423$, $0{\cdot}2585 \le z \le 0{\cdot}2785$.

(viii) To a good approximation the distance N—C(3) (~3·81 Å) and its z component (~3·71 Å) do not change on passing from the δ phase (182 K, Depmeier & Mason, 1978) to the average structure of the ε phase at 130 K. On average the all-*trans* conformation of the PAM groups and their orientation are therefore maintained.

(ix) By way of contrast, the c-lattice parameter decreases by 0·17 Å (~0·7%). The difference is largely accounted for by the diminishing z distance (by partial interpretation) between C(3) atoms of two adjacent strata (1·024 Å for δ-PAMC, but 0·946 Å for ε-PAMC; the difference contributes twice to the reduction in c).

Observation (vi) follows directly from the application of the $(\frac{1}{2}-x, \frac{1}{2}+y, z, \frac{1}{2}+t)$ and $(\frac{1}{2}+x, y, \frac{1}{2}-z, t)$ superspace-group symmetry operations to the x-component modulation wave of the C(3) atoms. Symmetry arguments of this kind, however, neither lend themselves to providing explanations for the relative degree of certain displacements, nor do they explain why these structural distortions actually occur. In the following paragraphs we will offer an explanation for the observations listed above. In order to do so some structural characteristics of PAMC have to be recalled briefly. For the detailed descriptions of the various aspects of the structure of PAMC the reader is referred to the cited literature.

We note that a necessary condition for the realization of space group *Abma* in PAMC and, hence, of the m_y mirror planes, is a perfect librational movement of the PAM groups across these planes (flipping), resulting in equal probabilities for both sides, on the time scale of the diffraction experiment. Then we realize that N and Cl(2) atoms, being related as described in (i), are joined together by N—H(2)···Cl(2) hydrogen bonds. On average, the N and Cl(2) atoms are kept on the m_y mirror planes of δ-PAMC, because the attractive forces, which result from the hydrogen bonds on opposite sides of the mirror plane, cancel out. From the modulated N···Cl(2) distances (i), and from prior knowledge of the mode of operation of hydrogen bonds in layered perovskites (see, for example, Depmeier, 1977), we conclude that observation (i) can be explained by assuming a modulation of the occupancy of the H(2) atoms, *i.e.* of the $-NH_3$ orientation. Shorter N···Cl(2) distances would be indicative of a higher probability of finding an H(2) atom, and thus of increased attractive forces between N and Cl(2) and *vice-versa*. The antiphase relationship mentioned in (i) follows immediately. The attractive action on a given Cl(2) atom is accompanied by an equivalent one, which is the result of the $(\bar{x}, \bar{y}, \bar{z}, \bar{t},)$ symmetry operation. It acts upon a Cl(2)′ atom at the opposite apex of the $MnCl_6$ octahedron, but pulls in the opposite direction along y. Thus, the combined

forces result in the reported $\pm 5°$ tilts about axes parallel to **a**.

Whereas the dynamical disorder of the hydrogen-bonding system and the librational movement of the alkylammonium groups are common features of the room-temperature phases of all members of the $(C_nH_{2n+1}NH_3)_2MnCl_4$ family ($n < 10$), there is a unique structural aspect germane to PAMC. It concerns the region about $z \simeq 0{\cdot}25$, where terminal methyl groups [C(3) atoms] of adjacent layers (z and $\frac{1}{2}-z$) interlock, whereby additional relatively stable layers parallel to (001) and midway between $MnCl_6$ octahedral layers are formed (*cf.* Fig. 7 of Depmeier, 1979). These layers do not exist in the remaining members of the series. The idea has been put forward that the existence of these stable interlayers accounts for the majority of the unique properties of PAMC as compared with its homologues (Depmeier, 1979). This includes the extended thermal stability of PAMC as well as the occurrence of the modulated phases. We present here a scenario for the $\delta \rightarrow \varepsilon$ phase transition of PAMC, which relies strongly upon the existence of the stable interlayer. It provides consistent explanations for the observations described above.

Suppose a crystal of δ-PAMC is being cooled down. As the temperature decreases, the flipping rate of the PAM group slows down until a temperature of, say, 200 K is attained. Somewhere in this temperature range one would expect the proper freezing point of the reorientational disorder of the PAM groups, because for the ethyl homologue (EAMC) of PAMC, this transition happens at 225 K (Depmeier, 1977). However, this normal operation is prevented in PAMC by the existence of the unique interlayer at $z \simeq 0{\cdot}25$. It lowers the energy and thereby stabilizes the room-temperature phase of PAMC with respect to, *e.g.*, EAMC. Therefore, the PAM group and the hydrogen-bonding system continue their flipping, but as the temperature decreases further, the restoring forces diminish and the potentials become more and more anharmonic. The flipping frequency is probably already compatible with the time scale of neutron experiments, because strong critical scattering of the satellites of ε-PAMC, reaching far into the δ phase (up to $\sim$200 K), has been observed (Muralt, Kind & Bührer, 1988). At 165 K the ε phase becomes stable. The potentials for flipping of the PAM groups, with their associated hydrogen-bonding systems, are now really anharmonic with the ensuing tendency that the PAM groups prefer one of the two sides of the former m_y mirror planes. The consequently increased occupancy at one H(2) site attracts the neighbouring N and Cl(2) atoms along y. For these two atoms the attraction by the central H(2) results in the observed antiphase relationship of their longitudinal displacement waves along y (i). Neither x, nor z components are involved [(iii), (vii)]. Now we know from (viii) that the PAM groups largely preserve their conformation, as well as their projected length along z. The y displacement of the N atom must therefore be compensated by the C(3) atom. Because of (vii) this must happen in the xy plane.

Let us now look more thoroughly at the stable interlayer at $z \simeq 0{\cdot}25$ [see Fig. 7 of Depmeier (1979), *cf.* Depmeier & Mason (1978)]. One notices that this layer is composed of chains running along the x direction. The chains consist of methyl groups, alternately at height z and $\frac{1}{2}-z$, which are held together by tightly interlocked H(8) and H(9)′ atoms. Perpendicular to the chain direction, *i.e.* parallel y, the connection is much weaker. It is clear that a slip-by of these quite rigid chains will require less energy than their deformation. Therefore, in order to compensate for the displacements along y of the N atoms, the C(3) atoms do not move in the same direction, but rather react with a modulated slipping of the chains along the x direction (iii). Since the chains remain intact, all C(3) atoms must be in phase (vi). With N and C(3) being almost exclusively displaced along y and x, respectively, and depending on the extra condition (viii), these displacements have to be coupled in such a way that a maximum shift of N corresponds to a zero shift in C(3), and *vice-versa*. In other words, the two modulation waves must be in quadrature (v). Considering the rigidity of the PAM group and recalling that their extremes undergo almost pure x and y displacements, it can be realized immediately that the intermediate C(1) and C(2) atoms have to undergo combined x and y displacements (iv).

The mechanism described here implies that further decreases of temperature, and hence, further reduced flipping rates of the PAM group and the associated hydrogen-bonding system, will lead to more-pronounced differences between the occupancies of the H(2) and H(2)′ sites (related by m_y in the δ phase). This will then entail more distinct attractive forces acting upon N and Cl(2) and, therefore, larger modulation amplitudes for all parts of the structure will be the consequence. This will then become noticeable as higher intensities of satellite reflections. In fact, neutron experiments have revealed the strong increase of satellite intensities with decreasing temperature within the range of the ε phase of PAMC (Depmeier & Mason, 1982, 1983).

Thus our model consists of an 'undercooled' flipping motion of the PAM group and of the associated hydrogen-bonding system. It requires that the freezing is blocked by the existence of the stable interlayer at $z \simeq 0{\cdot}25$. Therefore the system is frustrated. In the sense of Heine & McConnell (1984) the system 'makes the best of a bad job' by making a compromise. This is the formation of an inter-

mediate incommensurately modulated phase. It is quite obvious that the structure has to undergo important alterations upon freezing. The final transition to the ζ phase at 112·5 K is indeed a very dramatic event, as demonstrated by neutron experiments (Depmeier & Mason, 1982, 1983). From observations of lattice parameters and intensities of main reflections, these authors concluded that this so-called lock-in-flip phase transition is indeed triggered by the freezing of the propylammonium ions. This opinion has been confirmed spectroscopically (Muralt, 1984).

The diffraction experiment was performed in the Institut für Kristallographie of the Universität Karlsruhe (TH). We thank Mr G. Mattern for his skillful technical assistance.

References

Brunskill, I. H. & Depmeier, W. (1982). *Acta Cryst.* **A38**, 132–137.

Depmeier, W. (1977). *Acta Cryst.* **B33**, 3713–3718.

Depmeier, W. (1979). *J. Solid State Chem.* **29**, 15–26.

Depmeier, W. (1986). *Ferroelectrics*, **66**, 109–123.

Depmeier, W. & Mason, S. A. (1978). *Acta Cryst.* **B34**, 920–922.

Depmeier, W. & Mason, S. A. (1982). *Solid State Commun.* **44**, 719–722.

Depmeier, W. & Mason, S. A. (1983). *Solid State Commun.* **46**, 409–412.

Heine, V. & McConnell, J. D. C. (1984). *J. Phys. C*, **17**, 1199–1220.

International Tables for X-ray Crystallography (1974). Vol. IV. Birmingham: Kynoch Press. (Present distributor Kluwer Academic Publishers, Dordrecht.)

Johnson, C. K. (1965). *ORTEP*. Report ORNL-3794. Oak Ridge National Laboratory, Tennessee, USA.

Muralt, P. (1984). *Two Unusual Incommensurate–Commensurate Phase Transitions in a Layer-Structure Compound.* Dissertation, ETH No. 7524, Zürich, Switzerland.

Muralt, P., Kind, R. & Bührer, W. (1988). *Phys. Rev. B.* In the press.

Sheldrick, G. M. (1978). *SHELXTL. An Integrated System for Solving, Refining and Displaying Crystal Structures from Diffraction Data.* Univ. of Göttingen, Federal Republic of Germany.

Steurer, W. (1987). *Acta Cryst.* **A43**, 36–42.

Willis, B. T. M. & Pryor, A. W. (1975). *Thermal Vibrations in Crystallography*. Cambridge Univ. Press.

Wolff, P. M. de, Janssen, T. & Janner, A. (1981). *Acta Cryst.* **A37**, 625–636.

Yamamoto, A. (1982*a*). *Acta Cryst.* **A38**, 87–92.

Yamamoto, A. (1982*b*). *REMOS*82. A computer program for the refinement of modulated structures. National Institute for Research of Inorganic Matertials, Sakura-mura, Niihari-gun, Ibaraki 305, Japan.

Acta Cryst. (1989). B**45**, 562–566

Hydrogen Bonding in 3-Azetidinol. I. Crystal and Molecular Structure

By Michael Gajhede

Department of Physical Chemistry, University of Copenhagen, Universitetsparken 5, DK-2100 Copenhagen, Denmark

and Uffe Anthoni, Carsten Christophersen and Per Halfdan Nielsen

Marine Chemistry Section, The H. C. Ørsted Institute, University of Copenhagen, Universitetsparken 5, DK-2100 Copenhagen, Denmark

(*Received* 2 *February* 1989; *accepted* 25 *May* 1989)

Abstract

C_3H_7NO, $M_r = 73·09$, orthorhombic, *Pnam*, $a = 7·799$ (4), $b = 5·729$ (14), $c = 8·241$ (4) Å, $V = 368·20$ (2) Å^3, $Z = 4$, $D_x = 1·318$ (1), $D_m = 1·33$ (1) g cm^{-3}, λ(Mo $K\alpha$) = 0·71073 Å, $\mu = 0·8$ cm^{-1}, $F(000) = 152$, $T = 110$ K, final $R = 0·034$ for 833 unique reflections. The conformations of azetidine rings vary considerably in different crystal structures. *Ab initio* calculations on 3-azetidinol predict that intermolecular hydrogen bonding has a significant effect on the conformation. The potential surface for changing the puckering angle of azetidines appears to be quite flat. The high melting point of 3-azetidinol is due to strong hydrogen bonding and possibly also antiparallel atomic group dipole moments in molecular stacks.

Introduction

Charamin, 4-azoniaspiro[3.3]heptane-2,6-diol, was recently identified as an antibiotic principle from the green alga *Chara globularis* (Anthoni, Nielsen, Smith-Hansen, Wium-Andersen & Christophersen, 1987). Charamin was prepared synthetically *via* 3-azetidinol making the latter precursor available for further study. As charamin bears a permanent charge, which prohibits gas-phase studies, 3-azetidinol was selected as a model for studying the detailed structural aspects of this new system in different phases. The structure

0108-7681/89/060562-05$03.00